Dynamic characteristics of nanoindentation in Ni: A molecular dynamics simulation study*

Muhammad Imran[a)], Fayyaz Hussain[a)b)†], Muhammad Rashid[a)], and S. A. Ahmad[a)]

[a)] *Department of Physics Simulation Lab, Islamia University of Bahawalpur* 63100, *Pakistan*
[b)] *Department of Physics, National University of Singapore* 117542, *Singapore*

(Received 10 May 2012; revised manuscript received 1 June 2012)

In this work, three-dimensional molecular dynamics simulation is carried out to elucidate the nanoindentation behaviour of single crystal Ni. The substrate indenter system is modelled using hybrid interatomic potentials including the manybody potential (embedded atom method) and two-body Morse potential. The spherical indenter is chosen, and the simulation is performed for different loading rates from 10 m/s to 200 m/s. Results show that the maximum indentation load and hardness of the system increase with the increase of velocity. The effect of indenter size on the nanoindentation response is also analysed. It is found that the maximum indentation load is higher for the large indenter whereas the hardness is higher for the smaller indenter. Dynamic nanoindentation is carried out to investigate the behaviour of Ni substrate to multiple loading-unloading cycles. It is observed from the results that the increase in the number of loading unloading cycles reduces the maximum load and hardness of the Ni substrate. This is attributed to the decrease in recovery force due to defects and dislocations produced after each indentation cycle.

Keywords: indentation, nanocrystalline, loading-unloading, dislocation

PACS: 62.23.–c, 62.20.F–, 62.20.mt **DOI:** 10.1088/1674-1056/21/11/116201

1. Introduction

Nanoindentation is the most promising technique frequently used to study the mechanical behaviour of the material at nanoscale. Commonly hardness and elastic modulus are calculated from the data of the indentation process. When an indenter enters into the surface, the substrate starts to deform elastically up to a point where sufficiently high pressure has been established and plasticity sets in. This depth is characterized by a critical stress, with which the dislocation propagation starts.[1−3] Immense work has been reported to investigate various aspects of interaction between the indenter tip and the substrate, including the investigations of the adhesion of substrate atom with indenter and substrate fracture,[4,5] the elastic and plastic contact behaviour,[6] and the phase transformation.[7] Atomistic simulations have been performed for the investigation of incipient plasticity and defect nucleation under nanoindentation.[8] The explanation of indentation size effects for very shallow indentations showed that the indentation hardness decreased with the increase of depth irrespective of increasing or reducing strain gradients.[9] An atomistic simulation was performed to investigate the influence of the pre-existing stress on the indentation results at nanoscale.[10] Recently, a series of nanoindentation experiments has been reported to study the fracture toughness model of brittle films over the ductile substrates using the indentation technique.[11] Nanoindentation was simulated to understand the effect of twin boundaries parallel to the indented surface of (111) film. Twin boundaries appear as an effective obstacle to the dislocation propagation that dominates the deformation process resulting in film hardening.[12] Deformation induced grain growth in Ni film reported during the nanoindentation experiment was found to be thermally activated.[13] Hardness was found by measurement to be significantly dependent on the indentation size and the substrate for both hard and soft films.[14,15]

Molecular dynamics (MD) simulation has proved to be a well-established method to investigate the nanoindentation induced deformation mechanisms inside a crystal during plastic deformation.[16] Atomistic simulation has been performed to elucidate nanoindentation induced plasticity in Ni coatings deposited over copper specimens. Several deformation mechanisms such as dislocation pile up, cross slip, and movement of misfit dislocation were observed.[17] The MD

*Project supported by HEC, Pakistan.
†Corresponding author. E-mail: fiazz_hussain@yahoo.com
© 2012 Chinese Physical Society and IOP Publishing Ltd

simulation on single crystal Ni has been performed to analyse the dislocation nucleations in the different orientations and the elastic–plastic deformation at surfaces during the nanoindentation process.[18] The MD simulation was also performed to understand the mechanism of dislocation nucleation on Ni (001) during nanoindentation. The characteristic mechanisms favour the molecular models with and without a thermal layer. The tilt angles and the slip vector shapes of the indenter were investigated.[19] The MD simulation has been used effectively to elucidate the nanoscale machining process and the effects of different interatomic potentials, namely, the Lennard–Jonnes (LJ), Morse, and embedded atom method (EAM) potentials were analysed.[20] The simulation of nanoindentation into single Ni crystal was performed by using the quasi continuum method.[21] The MD simulation based on the EAM potential was employed to study the indentation response in Ni thin films of thicknesses at nanoscale.[22] A large-scale MD simulation was also performed for the study of material deformation in nanometric cutting.[23] Ni nanowires and thin films containing random distributions of nanoscale grains were subjected to spherical indentation using the MD technique, thereby suggesting a mitigation strategy for the sample boundary effects in nanoscale plasticity.[24]

Despite all the above mentioned facts, there are some other significant effects on the indentation behaviour of the material, which we are required to pay special attention to. In this work, we analyse the following points. (1) The first is the effects of indenter speed on the indentation response both in the elastic and the plastic regimes of Ni single crystal. (2) The size of indenter is also an important factor in the nanoindentation testing. The radius of the spherical indenter is gradually increased to observe size effects on the indentation response crystal. (3) Ni substrate is subjected to multiple loading-unloading cycles to investigate the response of Ni to the dynamic nanoindentation process. This simulation is based on classical MD. The purpose of this work is to provide further insight into the dynamic characteristics in Ni atoms during the nanoindentation mechanism.

2. Computational method

2.1. Sample preparation

The configuration of the simulated indenter and substrate is shown in Fig. 1. The substrate material is Ni having an fcc lattice with a lattice constant of 3.52 Å. The substrate sizes are 150 Å × 150 Å ×100 Å along the (1 1 −2), (1 −1 0), and (1 1 1) directions, respectively, containing 210151 atoms. A spherical diamond indenter (diameter = 60 Å) with (1 1 1) tip toward the substrate is used for the indentation process. The diameter is kept constant while observing the effects of velocity variation, however different values of diameter (40 Å, 60 Å, 80 Å, 100 Å, and 120 Å having 5907, 19965, 47291, 92189, and 159484 atoms, respectively) are used to analyse the indenter size effect on the indentation response of Ni crystal. Dynamic loading is performed to investigate the behaviour of single crystal Ni under multiple indentation cycles. For this purpose, a spherical rigid indenter with a diameter of 80 Å is chosen to perform multiple loading-unloading cycles up to a constant depth of 30 Å.

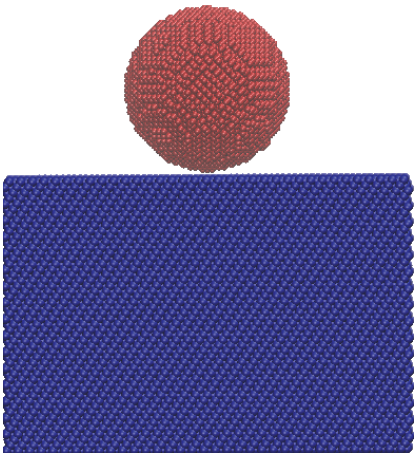


Fig. 1. (colour online) A typical simulation cell used for nanoindentation study.

2.2. Interatomic potential

Our computational cell consists of two types of atoms, C and Ni. There are three types of interactions possibly occurring between these atoms

(i) The interaction between Ni atoms is described by the well-known EAM potential reported in Refs. [25] and [26], where the total energy $E_{\rm tot}$ of this potential model can be calculated as

$$E_{\rm tot} = \sum F_i(\rho_{{\rm h},i}) + \frac{1}{2}\sum_i \sum_{j(\neq i)} \phi_{ij}(R_{ij}).$$

In this expression, $\rho_{{\rm h},i}$ is the electron density of the host atom i due to all atoms of the system, $F_i\,(\rho_{{\rm h},i})$ is the energy to embed atom into the background with electron density ρ, and $\phi_{ij}\,(R_{ij})$ is the core–core pair repulsion between atoms i and j separated by a distance R_{ij}.

(ii) The two-body Morse potential is employed to describe the interaction between C and Ni atoms, and it is extensively used in the MD simulation.[27] The Morse potential considers only the interaction between

two atoms without including the simultaneous influence of their neighbouring atoms. The Morse potential energy, $U_{\rm Morse}(r_{ij})$, can be described with three parameters as

$$U_{\rm Morse}(r_{ij}) = D[\,{\rm e}^{-2\alpha(r_{ij}-r_0)} - 2\,{\rm e}^{-\alpha(r_{ij}-r_0)}],$$
$$r_{ij} < r_c,$$

where D is the cohesive energy of exchange interaction, r_0 is the equilibrium distance, r_{ij} is the separation distance between atoms i and j. The α is fitted to the bulk modulus of the material. For C–Ni atoms, the values of D, α, and r_0 are 1.0094 eV, 0.19875 nm, and 0.256 nm, respectively.[19]

(iii) C–C atoms of the indenter are all taken to be rigid and treated as a single particle, hence the equation of motion for the individual atom should not be integrated to save simulation time.

2.3. Simulation process

A large-scale Atomic/Molecular Massively Parallel Simulator (LAMMPS)[28] is used to perform the simulation throughout this work. The bottom three layers of the substrate Ni are kept fixed, periodic boundary conditions are used along the sides of the substrate, whereas the upper part is subject to free boundary conditions. The diamond indenter sphere is treated as being rigid and is placed 3 Å above the top surface of the substrate. The force acting on the individual particle of the indenter is calculated by summing the force contributions from the surrounding atoms. The substrate is first relaxed to minimum energy using the conjugate gradient method. The temperature of the system is kept constant (300 K) using the velocity rescaling method. A time step 1 fs is chosen for time integration of Newton's equation of motion.

2.4. Visualization of defects

Underlying deformation mechanisms can be made understandable by identifying the location and type of the nucleated defects. In this study, the centro-symmetry parameter disorder is utilized to identify the defect type and location. As is well known, fcc Ni possesses centro-symmetry, i.e. each atom of the fcc lattice has an equal and opposite bond to its nearest neighbours. This centro-symmetry changes when the material is deformed plastically and can be measured using the centro-symmetry parameter (CSP) defined as[29,23]

$$\mathrm{CSP} = \sum_{i=1,6} [\boldsymbol{R}_i + \boldsymbol{R}_{i+6}]^2,$$

where $\boldsymbol{R}_i$ and $\boldsymbol{R}_{i+6}$ are the vectors or bonds corresponding to the six pairs of opposite nearest neighbours in the fcc lattice. Interior defects can be selectively visualized with a technique used in Ref. [29]. CSP values between three and six are typical for stacking faults and dislocation cores: the CSP value below this range indicates that atoms nearly in the perfect lattice sites are not displayed for visualization purposes and atoms with CSP values greater than six indicate the surface.

3. Simulation results

3.1. Velocity effect

Nanoindentation of Ni substrate is performed using MD, and the indenter is subjected to moving in the direction perpendicular to the (111) surface. The velocities of the indenter are set to be 10 m/s, 50 m/s, 100 m/s, and 200 m/s respectively. Although the velocities are very high as compared with those in experimental work, in MD, it is necessary to move the indenter at such a high speed to reasonably reduce the simulation time. The resulting load depth curve for each loading rate is shown in Fig. 2(a). Hardness is the resistance to local deformation and is an important mechanical property to be measured during nanoindentation. The hardness-depth curve obtained

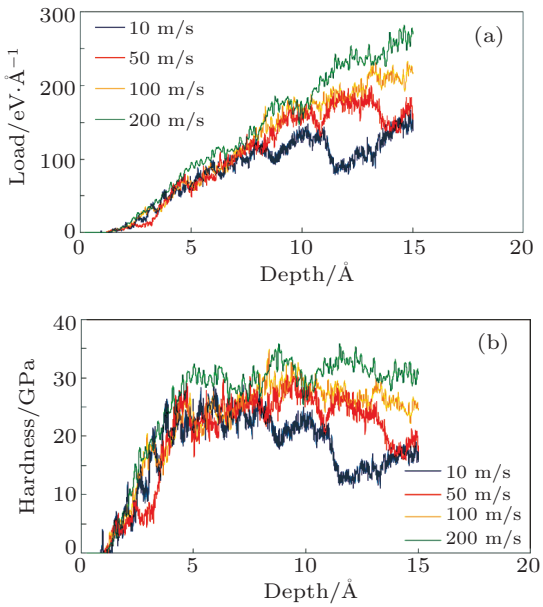


Fig. 2. (colour online) (a) Curves of load versus depth showing the variation of load with indenter velocity, and (b) curves of hardness versus depth exhibiting the variation of hardness with indenter velocity.

from the indentation process is shown in Fig. 2(b). Hardness is calculated using the following relation:

$$H = \frac{F_{\max}}{A_{\rm c}},$$

where $F_{\max}$ and $A_{\rm c}$ are the maximum indentation load and projected contact area, respectively. However, before the occurrence of the first yield point, the hardness–depth plot has no meaning. The erratic behaviour of the load–depth curve is due to a small variation in the contact area caused by the movement of bursts of dislocation toward the boundaries and the reflection from the fixed boundaries. A similar behaviour is also investigated in the previously reported work.[30]

It can be seen from the load displacement plot that for higher values of velocity, the slope of the load–displacement plot is steeper than that for the lower velocities. This also shows that hardness increases with the increase of the indentation rate, and this result is also consistent with Saha's experimental work.[31] At higher loading rates, the energy from the impact of the indenter is higher, which causes hardness and Young's modulus to increase at higher velocities. Typical defects and dislocations are produced during the nanoindentation process of the Ni substrate. These dislocations can be visualized individually on the basis of the value of CSP, whereas all the snapshots are taken using visual molecular dynamics (VMD) (http://www.ks.uiuc.edu). The pictures of different states of indentation at loading rate of 10 m/s are shown in Fig. 3, indicating that usually dislocations nucleate at the surface because surface atoms lose some of their neighboring atoms.

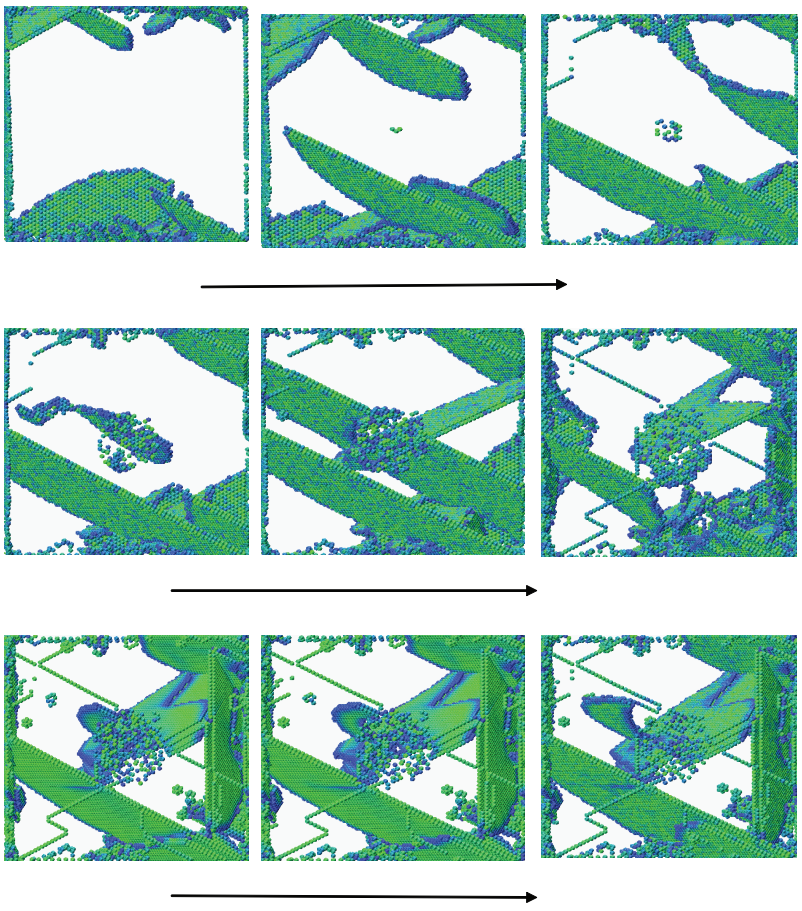


Fig. 3. (colour online) Defect evaluation during nanoindentation of Ni substrate at a loading rate of 10 m/s starting from indentation to maximum depth (1.5 nm). Defect includes edge dislocation, stacking fault, and dislocation movement due to the slip action of the adjacent atomic planes.

3.2. Effect of indenter radius

The effect of the indenter radius on the nanoindentation characteristics of single crystal Ni simulation is investigated using the indenters with different sizes (Diameter = 40 Å, 60 Å, 80 Å, 100 Å, and 120 Å). Basic simulation conditions are the same as

those discussed earlier. To analyse the nanoindentation response, the load displacement curve is drawn for the process in Fig. 4(a). It is clear that maximum indentation force is higher for the indenter with a larger diameter than that for the indenter with the smaller diameter. To analyse the hardness characteristics, the hardness–depth curve is shown in Fig. 4(b).

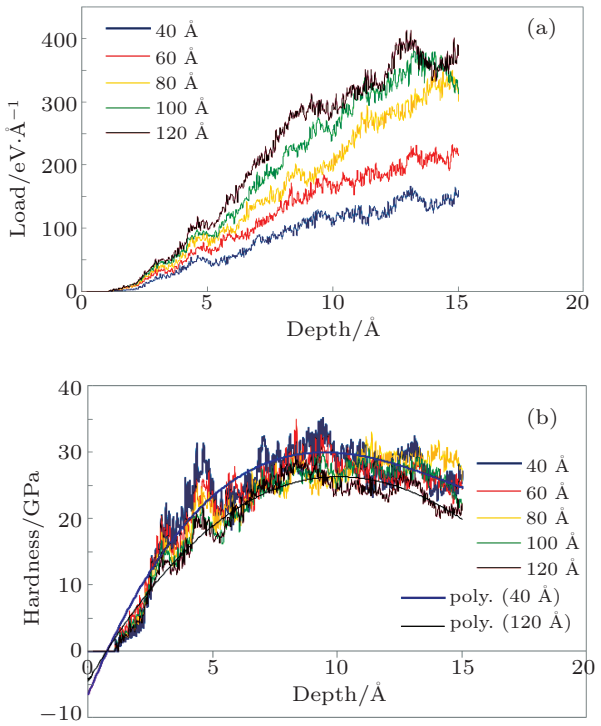


Fig. 4. (colour online) (a) Curves of load versus depth showing indenter size effects, and (b) curves of hardness versus depth exhibiting the significance of indenter size effects.

It is worth mentioning that contrary to the load–depth curve, the harness of the smaller indenter is higher than that of the larger indenter, as can be seen clearly from the trend lines of 40 Å and 120 Å diameters in the hardness depth plots. This is called the indentation size effect and is consistent with experimental observations in Refs. [32] and [33].

3.3. Dynamic loading and unloading response

MD simulation is performed to investigate the mechanical behaviour of Ni for dynamic multi-step nanoindentation. First the substrate is equilibrated at 300 K. An indenter with a diameter of 80 Å is subjected to moving at a velocity of 100 m/s in the direction perpendicular to the Ni (111) surface. During the first loading cycle, the indenter continues to move downward until it reaches its maximum depth (30 Å), which is constant for all the loading cycles. Then unloading starts until the indenter again separates from the surface atoms. The substrate is then allowed to recover for 3000 time steps; the Ni atoms show a large tendency to recover the adhesive forces present between the Ni atoms. The indenter is again set to be in motion for a second loading cycle, and the loading continues until the maximum depth is reached. Afterwards, the unloading starts, and the substrate freely recovers. Similarly a third loading and unloading cycle is performed in this way, and three indentation cycles are completed. To analyse the response of Ni (111) during the multi-step loading and unloading process, the load-time curve is plotted in Fig. 5.

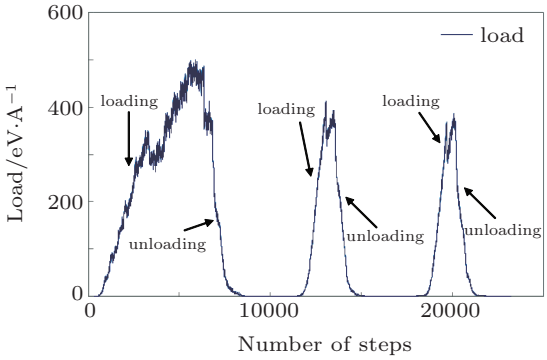


Fig. 5. (colour online) Curve of load versus time step, showing the effects of dynamic loading and unloading cycles.

It is clear from the load time step plot that at a maximum depth, the indentation force is higher in the first loading cycle and lower in the second loading cycle and it is lowest in the third cycle. This shows that the maximum force decreases with the increase of the loading-unloading cycle. Actually before indentation, there is a large adhesive force present between the Ni atoms. When the indenter moves into the substrate, it causes deformation in the substrate. When the substrate is unloaded, the elastic and adhesive forces start to recover in the vicinity of the indenter. Due to the deformed structure, the recovery forces are not so significant as before the indentation. Hence the resistance to the second loading cycle is lower than the first, and so is it for the third loading unloading cycle and vice versa. It shows that the defects and deformation produced after each indentation cycle are responsible for the decrease in the adhesive recovery forces. Hence an increase in the number of indentation cycles can reduce the maximum indentation force, under the condition of constant depth.

4. Conclusion

It is concluded that maximum load and hardness increase with the loading rate increasing. Dislocations are visualized using CSP values between 3 and 6, and pictures are taken to understand the dislocation mechanisms. It is clear that the maximum load is higher for the large size of indenter, whereas hardness–depth curves for different size indenters show that hardness is maximum for the smallest indenter and minimum for the largest one. The substrate is deformed during loading and recovered during the unloading process due to the adhesive and elastic forces present between these atoms. It is concluded that after each loading-unloading cycle, the resistance to deformation decreases due to the decrease in the recovery forces. The dislocations produced in the indentation process are responsible for the observed effects. So the increase of indentation cycles can reduce the hardness of the material.

References

[1] Ziegenhain G, Hermair A and Urbassek H M 2009 *J. Mech. Phys. Solids* **57** 1514

[2] Cripps F A C 2004 *Nanoindentation* (2nd edn.) (New York: Springer)

[3] Cripps F A C 2007 *Introduction to contact Mechanics* (2nd edn.) (New York: Springer)

[4] Landman U, Luedtke W D, Burnham N A and Colton R J 1990 *Science* **248** 454

[5] Li X and Bhushan B 1998 *Thin Solid Films* **315** 214

[6] Fang T H and Chang W J 2004 *Microelectron J.* **35** 595

[7] Cheong W C D and Zhang L C 2000 *Nanotechnology* **11** 173

[8] Lee Y, Park J Y, Kim S Y, Jun S and Im S 2005 *Mech. Mater.* **37** 1035

[9] Gerberich W W, Tymiak N I, Grunlan J C, Horstemeyer M F and Baskes M I 2002 *J. Appl. Mech.* **69** 433

[10] Schall J D and Brenner D W 2004 *J. Mater. Res.* **19** 3172

[11] Demidova N V, Wu X J and Liu R 2012 *Eng. Fract. Mech.* **82** 17

[12] Yuan L, Xu Z, Shan D and Guo B 2012 *Appl. Surf. Sci.* **258** 6111

[13] Prasad M J N V and Chokshi A H 2012 *Scripta Mater.* **67** 133

[14] Ma Z S, Zhou Y C, Long S G and Lu C 2012 *Int. J. Plasticity* **34** 1

[15] Peng P, Lio G, Shi T, Tang Z and Gao Y 2010 *Appl. Sur. Sci.* **256** 6284

[16] Begau C, Hartmaier A, George E P and Pharr G M 2011 *Acta Mater.* **59** 934

[17] Saraev D and Miller R E 2006 *Acta Mater.* **54** 33

[18] Kum O 2005 *Mol. Simul.* **31** 115

[19] Chang W Y, Fang T H, Lin S J and Huang J J 2010 *Mol. Simulat.* **36** 815

[20] Oluwajobi A and Chen X 2011 *Int. J. Auto. Comput.* **8** 326

[21] Jiuhui L, Xing Z, Shaoqing W and Caibei Z 2010 *Journal of Wuhan University of Technology-Mater. Sci. Ed.* June 423

[22] Nair A K, Gaudreau E P, Farkas D and Kriz R D 2008 *Int. J. Plasticity* **24** 2016

[23] Pei Q X, Lu C, Lee H P and Zhang Y W 2009 *Nanoscale Res. Lett.* **4** 444

[24] Sansoz F and Dupont V 2010 *Scripta Mater.* **63** 1136

[25] Foiles S M, Baskes M I and Daw M S 1986 *Phys. Rev.* B **33** 7983

[26] Daw M S and Baskes M I 1984 *Phys. Rev.* B **29** 6443

[27] Maekawa K and Itoh A 1995 *Wear* **188** 115

[28] Plimpton S J 1995 *J. Comput. Phys.* **117** 1

[29] Kelchner C L , Plimpton S J and Hamilton J C 1998 *Phys. Rev.* B **58** 11085

[30] Saraev D and Miller R E 2006 *Acta Mater.* **54** 33

[31] Saha R and Nix W D 2002 *Acta Mater.* **50** 23

[32] Gerberich W W, Tymyak N I, Grunlan J C, Horstemeyer M F and Baskes M I 2002 *J. Appl. Mech.* **69** 433

[33] Nix W and Gao H 1998 *J. Mech. Phys. Solids* **46** 411